Observations of the Near-Surface Internal Wavefield[1]

ROBERT PINKEL

University of California, San Diego, Marine Physical Laboratory, Scripps Institution of Oceanography, San Diego, 92152

(Manuscript received 9 February 1981, in final form 18 May 1981)

ABSTRACT

During January 1977 a cruise was conducted off the California coast on the Research Platform FLIP. Repeated temperature profiling devices were used to sense the internal wavefield in the top 400 m of the sea. From a sequence of 8192 profiles, vertical-velocity spectra and vertical coherence were calculated. Near-surface vertical coherence was found to increase with increasing frequency between local inertial and Väisälä frequencies. Below 200 m the coherence was approximately constant with frequency. The near-surface change in the vertical coherence patterns results from the selective attenuation of the longer vertical wavelengths as the surface is approached. From frequency-depth changes in the near-surface coherence, variations of the internal-wave spectral form can be inferred, in spite of the fact that the deep vertical coherence remains constant. This near-surface effect is not so apparent in data from horizontal-velocity sensors, as only the vertical component of motion is constrained to vanish at the sea surface.

1. Introduction

During January 1977 a cruise was conducted on the Research Platform FLIP to observe oceanic internal waves off the coast of California. A repeated CTD profiling system was used to sense the oceanic vertical-velocity field in the top 400 m of the sea. Twelve days of continuous data were obtained. It was planned to use this information to examine the combined wavenumber-frequency dependence of the internal-wave spectrum. Controversy over the form of the spectrum has existed since the earliest attempts to measure the internal wavefield. The discussion has become more focused since Garrett and Munk (1972a) introduced a model which facilitated the comparison of different types of data. They characterized the spectrum as simply as possible, assigning a scale bandwidth to the wavenumber dependence of the spectrum and discussing the frequency dependence of this bandwidth. Over the years a variety of views has emerged.

The drifting profiling measurements of Cairns (1975) and Cairns and Williams (1976) support the idea of a bandwidth independent of frequency, up to about 2–3 cph. The width corresponds to an excitation of 3–6 dominant modes. This view is supported by a variety of moored experiments, primarily using current meters or thermistors as sensors. Garrett and Munk (1975) have adopted this uniform bandwidth hypothesis into their model of the wave spectrum. From towed CTD and thermistor chain experiments, Katz has demonstrated general agreement with the model (Katz, 1975; Katz and Briscoe, 1979), while Nelson and Milder (1981), Bell (1976) and Paulson *et al.* (1980) have seen significant differences. Using estimates of coherence at fixed vertical separation as a function of horizontal wavenumber, they have produced a picture more consistent with an increase in vertical coherence (or decrease in vertical-wavenumber bandwidth) with increasing frequency. Pinkel (1975) has noted a similar tendency from his vertical profiling measurements. The IWEX data (Briscoe, 1975) support a picture of some 20 energetic modes at low frequency, decreasing to 10 at 2 cph (Müller *et al.*, 1978).

From the temperature profiles obtained in the 1977 FLIP experiment, time series of vertical velocity were calculated at many depths. The original plan was to estimate a two-dimensional wavenumber-frequency spectrum from these data. Prior to multi-dimensional spectral analysis, frequency spectra and vertical coherences were estimated at many depths to check for vertical stationarity. It was found that the proximity of the sea surface strongly influenced wavefield statistics. Deep vertical coherences were found to be approximately constant with frequency. Shallower estimates increased with increasing frequency.

This paper will document the changes in the internal wave spectrum as the surface is approached. The power spectrum and vertical coherence of the vertical velocity field will be discussed. The following notation is used:

z	depth
H_0	ocean depth

[1] *Contribution of the Scripps Institution of Oceanography, new series.*

0022-3670/81/091248-10$06.50

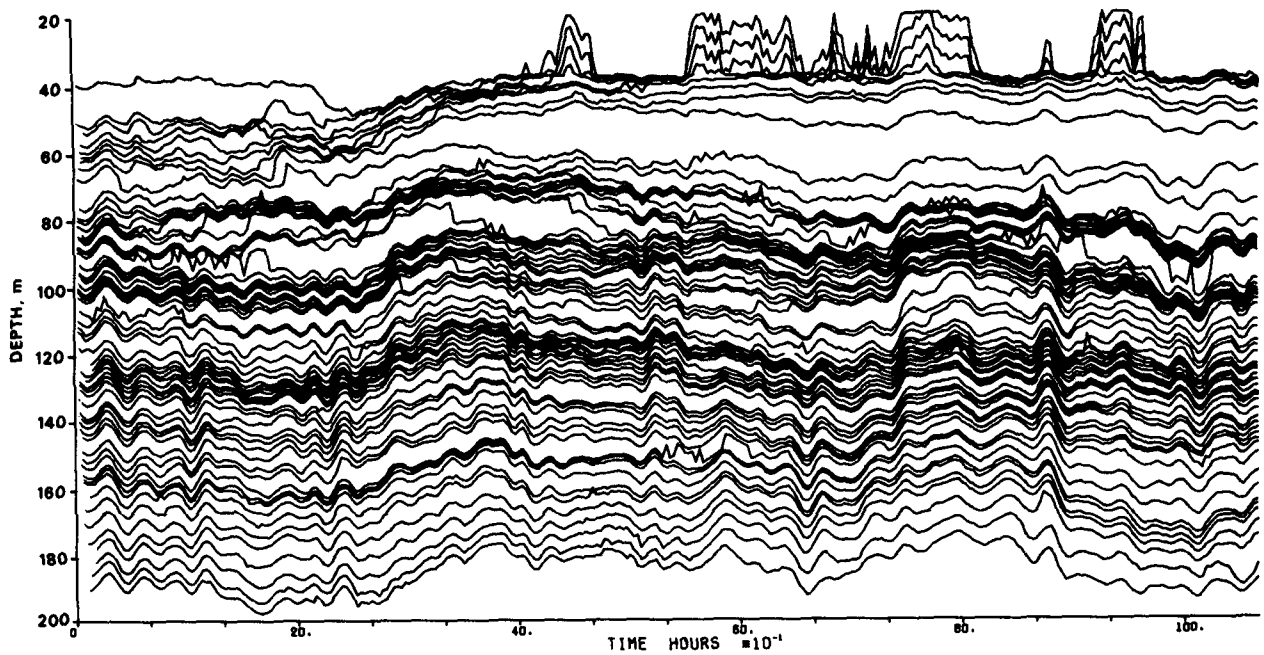

FIG. 1. Representative isotherm vertical displacement as a function of depth and time.

ω wave frequency
f local inertial frequency
$N(z)$ Väisälä frequency
$H(\omega)$ waveguide thickness as a function of frequency
k_z vertical wavenumber
k_H horizontal wavenumber.

2. Observations

The measurements to be discussed were taken from the Research Platform FLIP over a 12-day period in January 1977. During this time FLIP drifted westward ~70 km from 31°30'N, 122°10'W to 31°40'N, 122°50'W in response to light easterly winds. The instrumentation on board included wind and surface-swell sensors, a prototype Doppler sonar, three automatically profiling CTD arrays, and a slow profiling current meter array developed by Robert Weller of the Woods Hole Oceanographic Institution (Weller, 1981).

This paper deals with data from a single CTD profiling array: specifically, a sequence of 8192 consecutive temperature profiles of the top 400 m of the sea. The measurement system is discussed by Pinkel (1975) and Occhiello and Pinkel (1976). Each profiler consists of a pair of CTD's: one mounted at the end of a 400 m three-conductor well-logging cable, and the other 183 m up from the end. Each profiler cable is suspended from one of FLIP's three booms and is attached at the inboard end to a computer-controlled winch. The upper CTD starts each profile just below the sea surface and completes it at approximately 215 m depth. The lower sensors travel from 185 to 400 m. Profiles are repeated every 125 s. Some 700 profiles per day are collected from each array.

Traditionally, the internal-wave presence in repeated temperature profile data has been visualized by tracking the time fluctuations of a series of isotherm depths. Such a display is presented in Fig. 1. Here, 64 separate isotherms separated by ~0.10°C are followed over a 10 h period. Below 70 m, the dominant cause of isotherm motion is internal waves. High-frequency waves are seen to occur in groups of one to three crests which exhibit remarkable phase persistence with depth. Lower frequency motions have greater displacements and show greater phase variability with depth.

Above 70 m in this particular data segment, the isotherm motions are strongly influenced by the horizontal advection of water under FLIP. A secondary mixing (near-isothermal) layer intrudes at depths from 40 to 70 m during the 10 h period. Patches of cold fresh surface water drift by intermittently, causing the irregular jumps in the upper few isotherms. Such massive intrusions are rare during the cruise. For most of the operation the top of the thermocline is at ~60 m depth, with weak stratification above.

In the time series analysis of this data set, isotherm displacement is not used as the primary information. Over a period of many days isotherms near the upper and lower extremes of the observation interval tend to wander in and out of view. This interrupts the time series. Instead an equivalent purely Eulerian

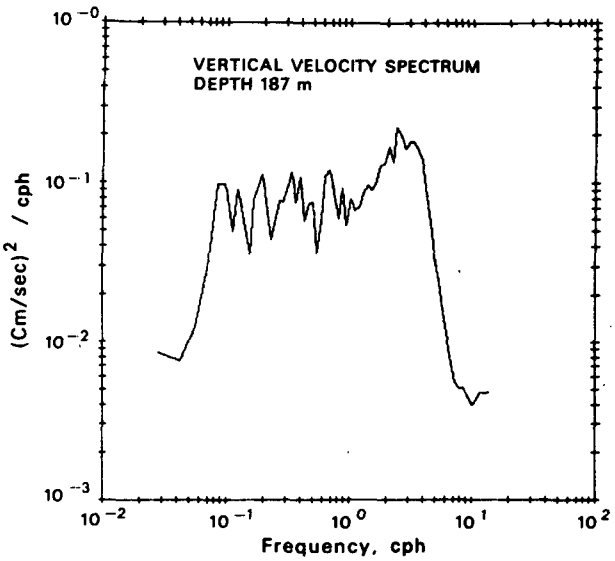

FIG. 2. Vertical velocity spectrum, logarithmically averaged.

data set has been produced. A set of 64 evenly spaced depths is selected, from 48 to 392 m. During each profile, the temperature at each of these reference depths is recorded. On the next profile, the depths at which these 64 temperatures are encountered are recorded. A new set of 64 temperatures is chosen at the reference depths. From the depth displacement observed, a mean vertical velocity over the 125 s interval between drops is calculated for each depth. Thus, time series of vertical velocity at fixed depths are produced. The time series have the attractive property that they are not "microstructure contaminated", even though fixed in depth. However, to the extent that the smaller scale components of the wavefield are vertically advected by larger scale motions such as the tide, fixed-depth observations introduce a nonlinearity to the measurement that does not appear in isotherm-following measurements.

3. Representative spectra and cross spectra—upper ocean

The time series of vertical velocity can be Fourier-transformed and averaged to produce power spectra at the different depths. A representative example is given in Fig. 2. The spectrum is logarithmically averaged, with 18 degrees of freedom in the lowest frequency band, 200 degrees in the highest. It is seen that spectral variance is confined between the local Väisälä and inertial frequencies. The spectrum is essentially flat between tidal frequency and 1 cph, with a series of irregular peaks that are of marginal statistical significance. Properly recolored, this spectrum would correspond to a displacement spectrum of ω^{-2} form between tidal frequency and 1 cph. Above 1 cph the spectrum rises to a pre-cutoff peak. This corresponds to the high-frequency waves visible in Fig. 1. With only a few crests per group in the time domain, $\Delta\omega/\omega$ is of order 1 in the frequency domain. It is thus not surprising to see that the spectral peak at 3 cph is ~3 cph wide.

The cutoff in the spectrum at the local Väisälä frequency indicates the role of stability in limiting wave propagation. Internal waves can only propagate through that region of the water column in which $N > \omega$. As the Väisälä frequency varies with depth, an internal waveguide is established of a thickness H that varies with frequency. The bottom boundary of the waveguide is set by the Väisälä profile for $\omega > N(H_0)$, or by the depth of the ocean for $\omega < N(H_0)$. The drifting float measurements of Voorhis (1968) were the first sensitive enough to detect this spectral cutoff. Fig. 2 is quite similar to the vertical-velocity spectrum in Voorhis' (1968) Fig. 6.

It is worthwhile to compare velocity spectra over many depths, as in Fig. 3. Here nine spectra from depths 147–193 m are plotted. The scale is appropriate for the shallowest spectrum. Deeper spectra are offset by successive −5 dB increments. The

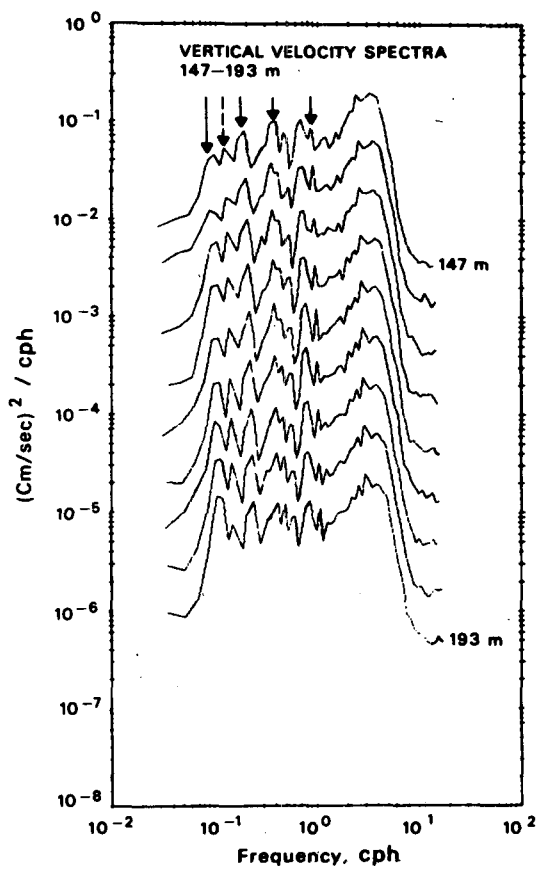

FIG. 3. Vertical velocity spectra. The scale for the uppermost spectrum is correct. Subsequent spectra are displaced by −5 dB. Solid arrows indicate the frequencies of the M2 tide and its first three harmonics. The dashed arrow marks the sum of inertial and tidal frequencies.

regularity of the lowest three spectral peaks is striking. The first peak is the semidiurnal tide. The frequency of the second peak is at the sum of tidal and inertial frequencies. The third peak is the first harmonic of the tide. Note that the power in the internal tide increases by a factor of 10 over the 46 m between the upper and lower measurements.

The vertical structure of both the harmonics and the continuum can be further examined through vertical coherence and phase spectra. Representative examples are presented in Fig. 4. The corresponding power spectra are seen in Fig. 3, top and second from bottom. The estimates are averaged logarithmically in frequency as in Fig. 3. Significant values of the coherence are seen between inertial and Väisälä frequencies. A high-coherence peak is found just before the Väisälä cutoff corresponding to the striking high-frequency wave groups seen in Fig. 1. The coherence also peaks at the tidal frequency and its first harmonic. In contrast, there is a local coherence minimum at the sum of inertial and tidal frequencies.

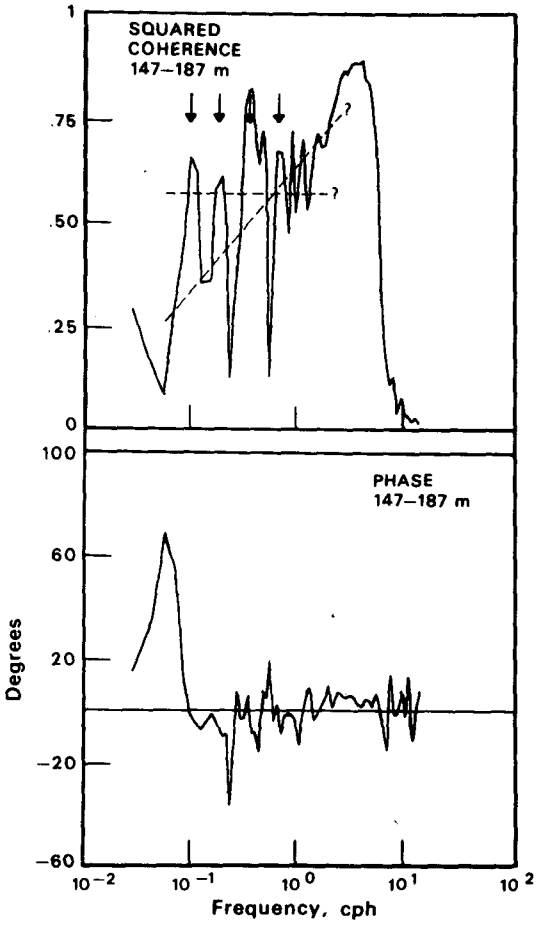

FIG. 4. Vertical squared-coherence and phase, 36 m vertical separation. The frequencies of the M2 tide and its first three harmonics are indicated by the vertical arrows.

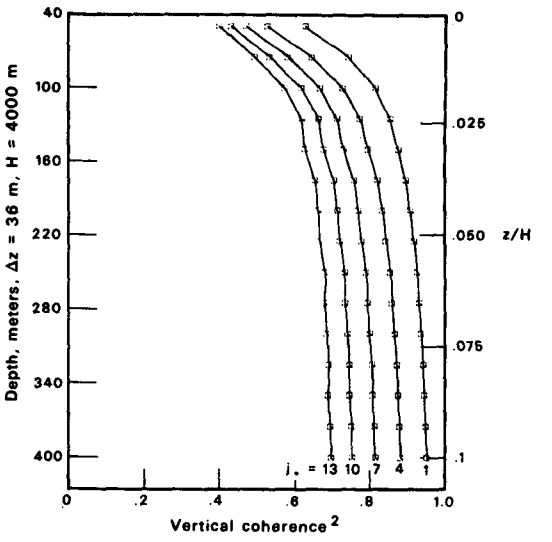

FIG. 5. Numerical simulation of the near-surface effect on the vertical coherence of vertical motion. A Garrett-Munk (1975) distribution of sine-wave "modes" is used for this constant-N study. The 36 m vertical coherence is given as a function of depth, for a 4 km ocean, in the left-hand ordinate. The right-hand scale gives dimensionless depth z/H, for the corresponding special case where $\Delta z/H = 0.009$.

The phase spectrum is not statistically different from zero except for a slight phase lead (~3°) between 3 and 7 cph. This lead is a result of the ~10 s time delay between the sampling of the upper and lower time series. The delay results from the finite (4 m s^{-1}) fallspeed of the profiler.

It is tempting to conclude from Fig. 4 that the vertical coherence of the internal wavefield in fact increases significantly as frequency increases, with the notable exception of obviously forced motions. However, when the coherence estimates are repeated at greater depths, a different, less convincing picture is obtained. The proximity of the sea surface is playing a role in these vertical coherence estimates.

4. Near-surface effects

The vertical motion of the internal wavefield is constrained to vanish at the sea surface. The rate at which vertical motion increases with depth depends on the vertical wavelength of the contributing waves. Thus, if one hypothesizes an internal wave spectrum that is essentially red in vertical wavenumber at depth, the contribution to the local variance becomes progressively whiter as the surface is approached. This results in diminished near-surface vertical coherences.

The effect can be modeled by assuming a specific vertical-wavenumber spectral form and calculating the corresponding vertical coherence at many depths. This is done in Fig. 5 using the Garrett-Munk 1975 spectrum and assuming a constant-N ocean. Near the surface, suppression of the energetic low

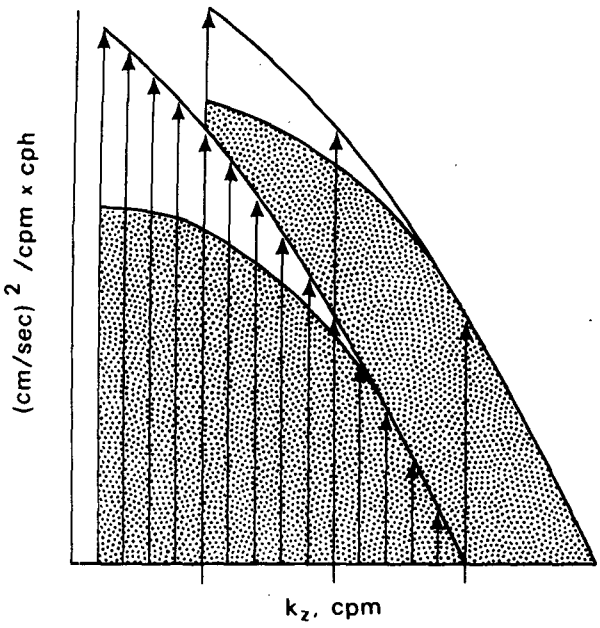

FIG. 6. Schematic illustration of the effect of waveguide thickness on near-surface vertical coherence. Vertical-wavenumber spectra are drawn at two frequency bands, at frequencies such that the thicknesses of the waveguides differ by a factor of 5. The upper boundary of the waveguide is assumed to be at the surface for both frequencies. Away from the surface the form of the spectrum is assumed to be the same at both frequencies, resulting in identical deep coherences. At a depth near the surface the contribution to the local variance is given by the shaded region. The near-surface vertical-wavenumber spectrum is whiter for the thick waveguide than for the thin. The near-surface coherence will be correspondingly lower.

modes leads to an effective broadening of the vertical-wavenumber spectrum, resulting in decreased coherence in the upper 200 m (assuming a 4 km deep ocean). For the Garrett-Munk spectrum, the ratio of deep to shallow coherence is not sensitive to the spectral bandwidth, as specified by their parameter j_*. For different spectral forms the relative coherence reduction can be expected to be different. The deep coherence will always be an indicator of the gross bandwidth of the spectrum. However, near-surface variations provide additional information on the exact spectral form.

It is important to emphasize that the near-surface coherence reduction is a function of both the form of the deep vertical-wavenumber spectrum and the ratio of observation depth z to overall waveguide thickness $H(\omega)$. It is perhaps most natural to interpret Fig. 5 in terms of the depth variability of near-surface vertical coherence. However, variations in waveguide thickness with frequency produce corresponding variations in the vertical coherence at a fixed near-surface depth.

This viewpoint is illustrated schematically in Fig. 6. Vertical wavenumber spectra are sketched for two cases where the waveguide thicknesses differ by a factor of 5. The upper solid curves outline the form of the deep spectra, which are assumed to be identical. The corresponding mid-waveguide vertical coherences are also identical. Vertical arrows represent the wavenumbers of the normal modes of the waveguides. At a fixed near-surface depth the contribution to the local variance is indicated by the shaded regions. The near-surface spectrum is locally whiter when the waveguide is thick (left) than when it is thin. The corresponding near-surface vertical coherence is lower. As waveguide thickness typically decreases with increasing frequency, a frequency-dependent near-surface signature can be expected.

In the January 1977 data, near-surface vertical-coherence variations are seen both at frequencies $\omega > N(H_0)$, where the waveguide thickness is changing with frequency, and at lower frequencies. The low-frequency signature is described next, followed by a discussion of waveguide-dependent effects.

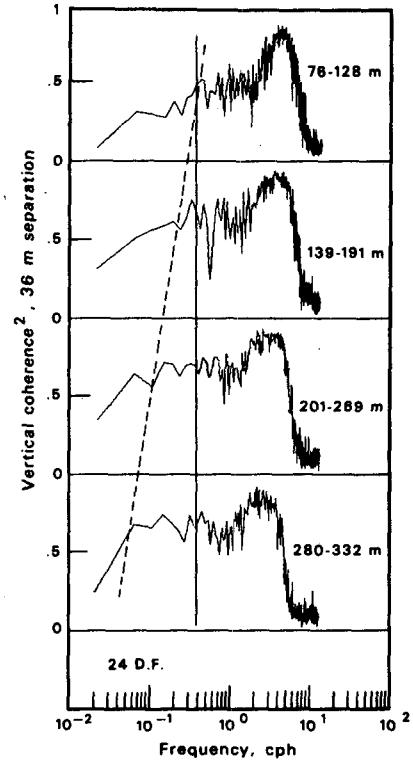

FIG. 7. 36 m squared coherence as a function of frequency for four depth zones. The frequency bandwidth is 1/24 cph. Energy in the M2 tidal frequency and its harmonics has been removed in these estimates. The near-surface coherence increases uniformly with increasing frequency up to $\omega \approx N(H_0)$. Deep coherences are greater, and approximately constant with frequency. The transition between these contrasting forms is illustrated schematically by the dashed line. As frequency increases above $\omega \approx N(H_0)$ the coherences reflect the changing thickness of the waveguide. These changes are seen from an alternative viewpoint in Fig. 9.

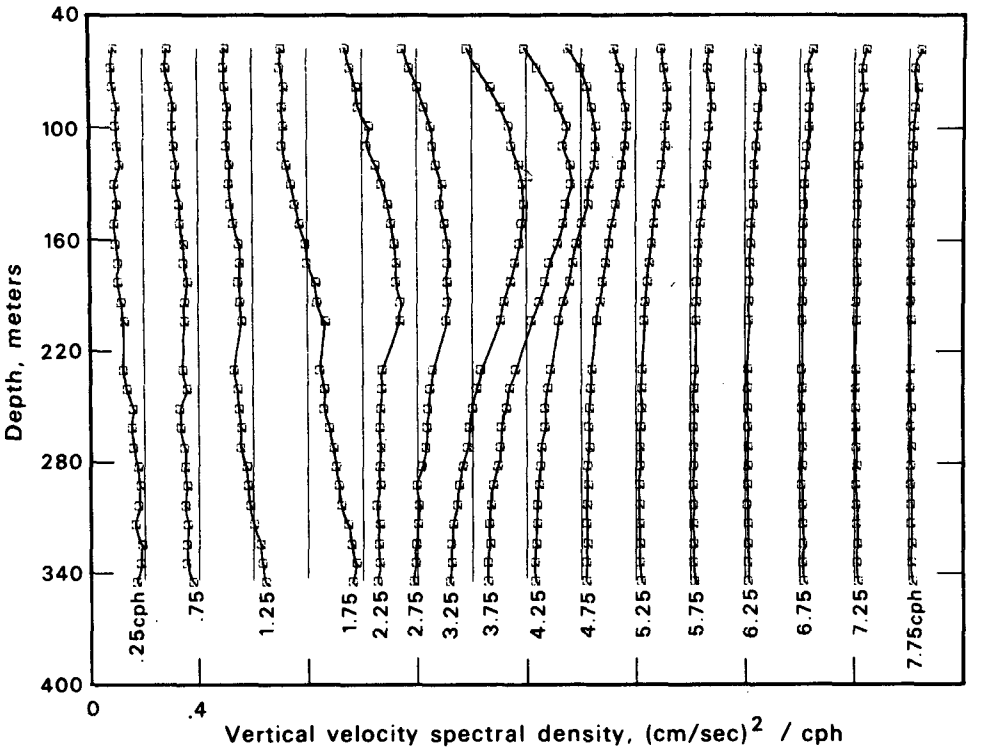

FIG. 8. Vertical-velocity spectral profiles, 0.5 cph bandwidth, 1152 degrees of freedom. The variance scale applies to the 0–0.5 cph profile. Subsequent profiles are displaced by 0.2 cm^2 s^{-2} cph^{-1}.

5. Low-frequency coherence variations

The discussion of near-surface effects was motivated by the observation that the coherence pattern of Fig. 4 changed as a function of depth. This is seen in Fig. 7, where coherence estimates are presented for four depth zones: 76–128, 189–191, 201–269 and 280–332 m. The estimates are calculated at 24 degrees of freedom, corresponding to $\frac{1}{24}$ cph resolution. The 12.4 h tide and its first three harmonics have not been included in the spectral and cross-spectral averages used to produce this figure in order to reduce the obvious tidal influence seen in Fig. 4. Spectral variance in bands of ±0.0035, ±0.007 and ±0.010 cph about the respective harmonic frequencies has been neglected. The vertical reference line denotes the approximate value of the Väisälä frequency at the sea floor, $N(H_0)$.

The deep coherences are essentially constant with frequency below ~1 cph, consistent with the picture adopted by Garrett and Munk. Above 1 cph there is a pre-cutoff peak, followed by a rapid drop in the coherence at the Väisälä frequency. The near-surface coherence pattern is similar to that of Fig. 4, without the peaks associated with the tide and its harmonics. The biggest differences, deep to shallow, are seen at frequencies below $N(H_0)$. The transition from the basically flat deep coherence pattern to the sloping shallow pattern is illustrated schematically by the slanting line. As waveguide thickness is constant with frequency, the wavenumber spectral form must be changing. The change is effected such that the deep coherence remains constant while shallower estimates increase with increasing frequency.

6. High-frequency coherence variations

At frequencies above $N(H_0)$ and below the pre-cutoff peak, the squared coherences in Fig. 7 appear approximately constant with frequency. The constant value decreases from 0.7 in the 280–332 m region to 0.4 in the 76–128 m zone. In part this is due to the variation in the Väisälä frequency with depth, which stretches the vertical scale of the wavefield with respect to the fixed 36 m depth separation. However, the near-surface effect also is playing a role.

It is convenient to try to separate these different influences by examining vertical profiles of the power spectrum and coherence in a set of fixed frequency bands. These are presented in Figs. 8 and 9. Data are averaged into ½ cph bands to form spectral estimates with 1152 degrees of freedom. No vertical smoothing is employed.

The dominant signature in the spectral profiles (Fig. 8) is the response of the wavefield to changes

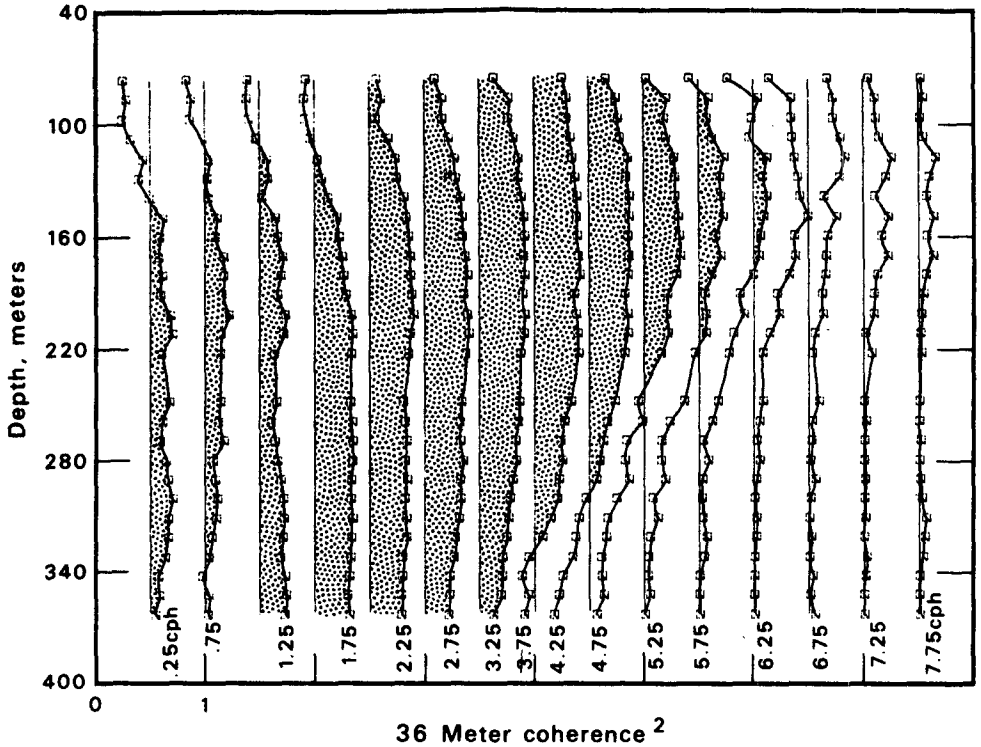

FIG. 9. Profiles of 36 m squared coherence, 0.5 cph bandwidth, 1152 degrees of freedom. The scale applies to the 0–0.5 cph band. Subsequent profiles are displaced by ½. The shading indicates the depth interval in which the squared coherence exceeds 0.5.

in waveguide thickness and Väisälä frequency. There is a small steady increase in vertical velocity variance with depth in the lowest frequency band. The increase is far greater in the fourth band (1.75 cph). In subsequent higher frequency bands a maximum in the variance appears, tracing out the thinning of the waveguide with increasing frequency.

The vertical squared-coherence profiles (Fig. 9), behave similarly. As the waveguide narrows, values of the coherence increase. The largest coherence values are in the 3.75 cph band. At this frequency the waveguide is only 400 m thick.

The near-surface coherence reduction is seen in the lower frequency profiles. This is visualized by tracking the depth at which the squared coherence equals 0.5 as a function of frequency. This depth increases as frequency decreases, in correspondence with the thickening waveguide. The pattern is not due to WKB effects resulting from depth changes in the Väisälä frequency. WKB effects would be more pronounced at higher rather than lower frequencies.

It is of interest to interpret these coherence profiles in terms of the equivalent number of energetic modes in the wavefield at each frequency. If it is assumed that the number of energetic modes is constant with frequency, the vertical coherence is a function of the ratio of vertical separation to waveguide thickness. As the waveguide thins with increasing frequency the coherence *at fixed separation* should drop. In fact, the coherence rises. When the data are properly stretched in the WKB sense the coherence increase at high frequency is reduced, but not eliminated. It appears that the number of energetic modes in the wavefield decreases markedly as the waveguide narrows. The decrease is effected such that the vertical coherence at fixed separation is approximately constant.

7. Discussion

Changes in the vertical wavenumber spectrum have been inferred from changing near-surface vertical-coherence patterns at low frequency and changing waveguide thickness at high frequency. In both cases the spectrum changes such that the deep vertical coherence remains approximately constant, for frequencies below the pre-cutoff peak. It seems as if the value of the deep coherence is more fundamental than either the number of energetic modes in the spectrum or the detailed spectral form.

It is of interest to display the vertical coherence estimates in equivalent dimensional terms to permit comparison with other relevant environmental features. An equivalent horizontal-wavenumber bandwidth can be introduced. Vertical coherence data

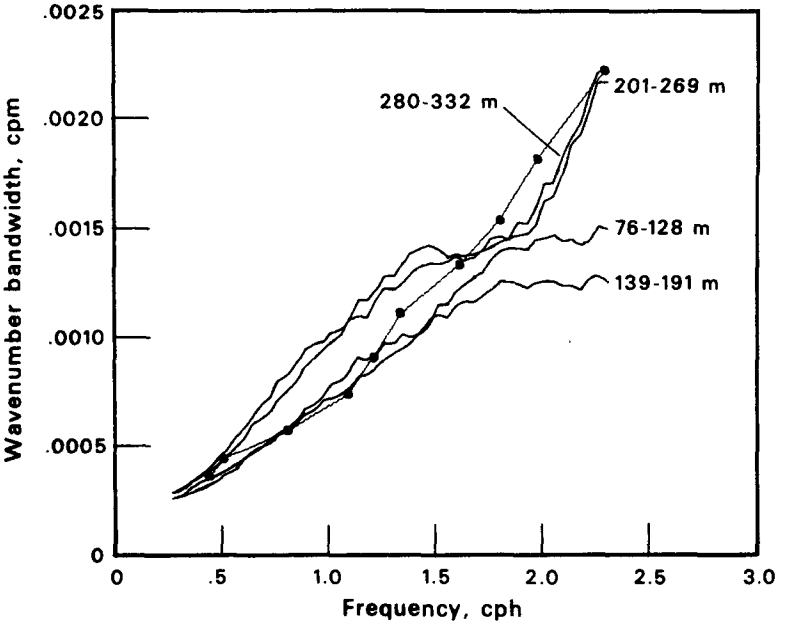

FIG. 10. The equivalent horizontal-wavenumber bandwidth of the wavefield as a function of frequency. The vertical coherence data of Fig. 7 are used to produce this plot. If it is assumed that the lower boundary of the energetic wavenumber band is at zero wavenumber, the lines trace the wavenumber of the upper boundary. The corresponding cutoff horizontal phase velocity is of the order 25–35 cm s^{-1}. The circled line gives the inverse waveguide thickness as a function of frequency, obtained from CALCOFI historical data.

are first used to estimate the vertical-wavenumber bandwidth of the spectrum. These estimates are then converted to horizontal-wavenumber bandwidths using WKB scaling.

The relationship between coherence and bandwidth can be obtained from the spectral definition of coherence:

$$R(\omega, \Delta z) = \frac{\int_{-\infty}^{\infty} S(\omega, k_z)\cos(k_z \Delta z)dk_z}{\int_{-\infty}^{\infty} S(\omega, k_z)dk_z},$$

$$\approx 1 - \frac{\tfrac{1}{2}\Delta z^2 \int_{-\infty}^{\infty} k_z^2 S(\omega, k_z)dk_z}{\int_{-\infty}^{\infty} S(\omega, k_z)dk_z}.$$

Defining

$$\Delta k_z^2 \equiv \frac{\int_{-\infty}^{\infty} k_z^2 S(\omega, k_z)dk_z}{\int_{-\infty}^{\infty} S(\omega, k_z)dk_z},$$

we have $\Delta k_z = (\sqrt{2}/\Delta z)[1 - R(\omega, \Delta z)]^{1/2}$. Note that Δk_z as approximated is in fact the second moment of the wavenumber spectrum. Δk_z has the interpretation of a bandwidth only if one assumes that the spectrum is red. The associated scale horizontal-wavenumber bandwidth is

$$\Delta k_H = \Delta k_z\{[\omega^2 - f^2]/[N^2(z) - \omega^2]\}^{1/2}.$$

This quantity is plotted as a function of frequency in Fig. 10 for the four depths considered in Fig. 7. To the extent that the four curves do not collapse into a single line, the WKB restretching is inaccurate. The curves would be more similar "unstretched", with a single value of the Väisälä frequency used for all. The general linearity of the curves suggest that a scale horizontal phase velocity, rather than a scale mode number is the more relevant index of spectral bandwidth in the frequency region where the waveguide thickness is rapidly changing.

As an interesting observation, a second type of data is included in Fig. 10. At each frequency, the inverse thickness of the internal waveguide $1/H(\omega)$ is plotted as the dotted line. CALCOFI data from July 1965 at 30°21.5'N, 119°28'W are used for the deep Väisälä-frequency information. The scale phase velocity defined by the curve agrees rather well with the bandwidth estimates produced from the profiling data. The product of waveguide thickness and horizontal wavenumber bandwidth is seen to be a constant of order 1, independent of frequency.

If this relationship is taken as a fundamental principle, then it should be possible to predict the Väisälä profile at all depths (the waveguide thick-

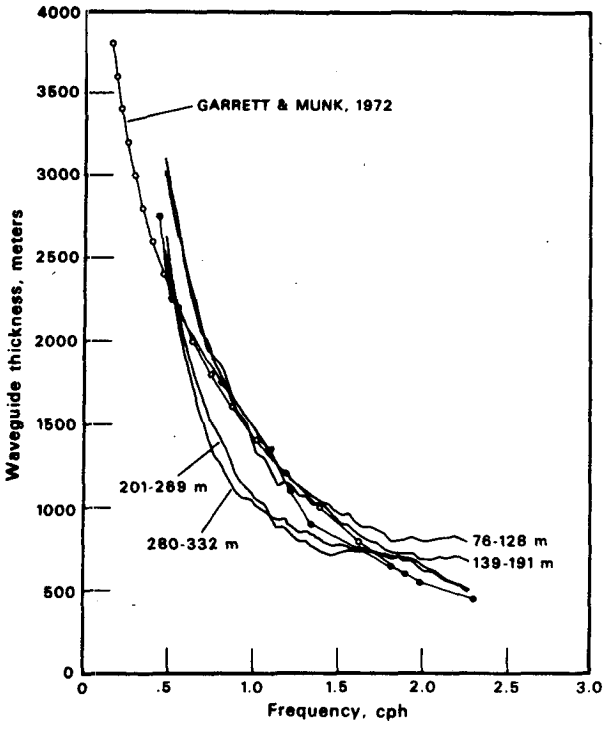

FIG. 11. Estimated waveguide thickness as a function of frequency. The assumptions here are that the inverse waveguide thickness is equal to the horizontal-wavenumber bandwidth, and that the Väisälä-frequency profile is a monotonic function of depth. The CALCOFI historical Väisälä-frequency profile is given by the closed circles. An exponential profile, suggested by Garrett and Munk (1972), is also given by the open circles.

ness as a function of frequency) from a single pair of upper ocean sensors. This is attempted in Fig. 11, where the inverse horizontal-wavenumber bandwidth of Fig. 10 is plotted versus frequency. The CALCOFI historical profile is plotted as a reference, along with the Garrett-Munk canonical exponential profile. As in Fig. 10, there are no adjustable parameters in the comparison. The similarity between the historical profile and the exponential one appears greater than between the inferred profile and the historical one. The scaling relations tend to force a profile of the form $N(z) = N_0/z$, which is biased only slightly by the particular coherence pattern measured by the sensors. Except at great depth and near the surface the oceanic profile is more nearly exponential.

8. Conclusions

From spectra and coherence estimates of isotherm vertical velocity, the evolution of the internal wavefield was observed in the top 400 m of the sea. Not surprisingly, the proximity to the sea surface, where vertical motion is constrained to vanish, strongly influenced the statistical patterns observed. A simple simulation suggests that the near-surface influence extends through the top 1/20 of the waveguide for a Garrett-Munk (1975) model of the wavefield with 1–13 energetic modes. The near-surface effect on the horizontal velocity field is much less significant than on the vertical field. Simple WKB-type scaling might better apply to near-surface horizontal-velocity data than to vertical-velocity data taken at the same depth and time. Also, since the waveguide-boundary effects depend on the fractional depth of the measurement (z/H), wavefield statistics can change with frequency near one boundary of the waveguide due to variations in depth of the other boundary, perhaps several kilometers below.

When looking at the historical controversy concerning the form of the internal wave spectrum, as outlined briefly in the Introduction, it becomes clear in retrospect that the various partisans can be segregated on the basis of the use of horizontal versus vertical displacement/velocity sensors and on the proximity of the measurements to the sea surface. The constancy of the deep vertical coherence with frequency implies that the vertical-wavenumber bandwidth of the spectrum does not vary appreciably. The exact spectral form changes, however, resulting in a frequency dependence in the near-surface coherence estimates. Detailed wavenumber-frequency spectral analysis will be necessary to resolve this changing form.

The measured vertical coherences can be represented by an equivalent horizontal-wavenumber bandwidth Δk_H. This bandwidth increases with increasing frequency, and is roughly equal to the inverse waveguide thickness. The interpretation is that the horizontal decorrelation scale (the inverse of Δk_H) is approximately equal to the waveguide thickness, for frequencies $N(H_0) < \omega \ll N_{\max}$. Alternatively stated, the product of the horizontal-wavenumber bandwidth and the waveguide thickness is a constant of order 1, independent of frequency. Attempts to stretch this finding, to predict the full-ocean Väisälä profile from upper ocean vertical-coherence measurements are only marginally successful.

The vertical coherence of the tide and its harmonics is greater than that of the near-surface continuum. Energy at the sum of tidal and inertial frequencies has lower coherence. These harmonics are easily seen and isolated in time-series measurements, but cannot be easily distinguished in towed measurements.

Acknowledgments. The author would like to thank L. Occhiello, E. Slater, L. Tomooka, and W. Whitney for developing and operating the profiling equip-

ment. J. Reid provided the deep Väisälä-frequency data used in Figs. 10 and 11. Discussions with W. Munk were particularly helpful. This work was funded by the National Science Foundation, the Office of Naval Research Codes 480 and 220, and NORDA Code 540.

REFERENCES

Bell, T. H., 1976: The structure of internal wave spectra as determined from towed thermistor chain measurements. *J. Geophys. Res.*, **81**, 3709–3714.

Briscoe, M. B., 1975: Preliminary results from the tri-moored internal wave experiment (IWEX). *J. Geophys. Res.*, **80**, 3872–3884.

Cairns, J. L., 1975: Internal wave measurements from a mid-water float. *J. Geophys. Res.*, **80**, 299–305.

——, and G. O. Williams, 1976: Internal wave observations from a mid-water float, Part II. *J. Geophys. Res.*, **81**, 1943–1950.

Garrett, G. J. R., and W. H. Munk, 1972a: Space time scales of internal waves. *Geophys. Fluid Dyn.*, **2**, 225–264.

——, and ——, 1972b: Space-time scales of internal waves: A progress report. *J. Geophys. Res.*, **80**, 291–297.

Katz, E. J., 1975: Tow spectra from MODE. *J. Geophys. Res.*, **80**, 1163–1167.

——, and M. B. Briscoe, 1979: Vertical coherence of the internal wavefield from towed sensors. *J. Phys. Oceanogr.*, **9**, 518–530.

Müller, P., D. J. Olbers and J. Willebrand, 1978: The IWEX spectrum. *J. Geophys. Res.*, **83**, 479–500.

Nelson, K. W., and D. M. Milder, 1981: Spatial measurements of internal waves in the upper thermocline and their interpretation. *American Institute of Physics Proceedings on Nonlinear Properties of Internal Waves,* Bruce West, Ed. (in press).

Occhiello, L. M. O., and R. Pinkel, 1976: Temperature measurement array for internal wave observations. OCEANS'76, MTS/IEEE 1976 CH 1118-9 OEC, pp. 20E1–20E7.

Paulson, C. A., R. J. Baumann and J. Wagner, 1980: Towed thermistor chain observations in JASIN. Oregon State University, Ref. 80-14, School of Oceanography, 202 pp.

Pinkel, R., 1975: Upper ocean internal wave observations from FLIP. *J. Geophys. Res.*, **80**, 3892–3910.

Voorhis, A. D., 1968: Measurement of vertical motion and the partition of energy in the New England slope water. *Deep-Sea Res.*, **15**, 599–609.

Weller, R. A., 1981: Observations of the velocity response to wind forcing in the upper ocean. *J. Geophys. Res.*, **86**, 1969–1979.